Lifetimes and transition probabilities for low-lying yrast levels in ^{130,132}Te

D. Kumar,[1,2] T. Bhattacharjee,[1,2,*] S. S. Alam,[1,3] S. Basak,[1,2] L. Gerhard,[4] L. Knafla,[4] A. Esmaylzadeh,[4] M. Ley,[4] F. Dunkel,[4] K. Schomaker,[4] J. -M. Régis,[4] J. Jolie,[4] Y. H. Kim,[5] U. Köster,[5] G. S. Simpson,[6] and L. M. Fraile[7]

[1]*Variable Energy Cyclotron Centre, Kolkata 700 064, India*
[2]*Homi Bhabha National Institute, Training School Complex, Anushakti Nagar, Mumbai 400 094, India*
[3]*Government General Degree College, Chapra 741123, West Bengal, India*
[4]*Institut für Kernphysik, Universität zu Köln, 50937 Köln, Germany*
[5]*Institut Laue-Langevin, 38042 Grenoble, France*
[6]*LPSC, Université Grenoble-Alpes, CNRS/IN2P3, 38026 Grenoble, France*
[7]*Grupo de Física Nuclear & IPARCOS, Facultad de Ciencias Físicas, Universidad Complutense - CEI Moncloa, E-28040 Madrid, Spain*

(Received 28 September 2021; revised 6 July 2022; accepted 1 September 2022; published 14 September 2022)

Lifetimes have been measured for the low-lying yrast levels of ^{130,132}Te using $\gamma-\gamma$ fast timing methods. The excited states were populated in β^- and IT decay of fission fragments, mass-separated by the Lohengrin separator at Institut Laue-Langevin. Four $LaBr_3$(Ce) detectors, placed at the focal plane of the spectrometer, were used for the $\gamma-\gamma$ fast timing measurement. Lifetimes of μs isomers were measured using coincidence of an ionization chamber with two Clover HPGe detectors. The measured lifetimes and absolute transition probabilities are discussed in the light of systematics with the neighboring nuclei. Large basis shell model calculations have been performed to interpret the level structure and transition probabilities in these even mass Te isotopes.

DOI: 10.1103/PhysRevC.106.034306

I. INTRODUCTION

Nuclear structure studies around doubly magic ^{132}Sn are of contemporary interest and are being explored with different experimental techniques [1–3]. One of the key focuses is on the measurement of transition probabilities for the low-lying levels [4–6], as this provides direct insight into the nucleon-nucleon interactions. Systematic measurements in even-even Te nuclei, having two protons above the $Z = 50$ shell closure, are useful to understand the evolution of nuclear structure between two extreme double shell closures of ^{100}Sn and ^{132}Sn, respectively. In this context, the measurement of nuclear level lifetimes becomes important and can be performed with the use of an appropriate γ-γ fast timing method [7,8]. The neutron-rich isotopes of Te, with few neutrons away from $N = 82$, can be populated with fission reactions and decay spectroscopy measurements can be carried out after separation of fission fragments in either or both of nuclear charge (Z) and mass (A).

The even-even Te isotopes show consistent vibrational structure having E_4^+/E_2^+ ratios close to 2.0 between $N =$ 50–82 [9–11]. The $B(E2)$ values, for both $10^+ \rightarrow 8^+$ and $2^+ \rightarrow 0^+$ decays, increase with increasing number of neutron holes around the $N = 82$ shell closure [10]. This increase in $B(E2)$, in case of even mass Te isotopes, was conjectured as the effect of configuration mixing with pure two-proton structure in neighboring even Sn isotopes. An unusual behavior was observed in the trend of transition rates around $N = 82$ as $B(E2)(2^+ \rightarrow 0^+)$ for $N = 80$ Te appeared to be higher compared to that at $N = 84$ [12]. This was explained with reduced neutron pairing beyond $N = 82$ in Ref. [13] but was resolved with new measurements and shell model calculations in the recent work of Ref. [5]. Systematic measurements of transition probabilities and their evolution are not available for all the low-lying levels in even mass Te isotopes below $N = 82$. This information would be of substantial importance to have a complete picture on the structural evolution as a function of angular momentum and changing neutron number up to the $N = 82$ shell closure.

Prior to the present work, in ^{130,132}Te, the lifetimes of the 10^+ levels were measured through the decay spectroscopy of μs isomers [10] and the $B(E2)$ of the $0^+ \rightarrow 2^+$ transition was measured through Coulomb excitation [12,14]. The level lifetimes of 6^+ and 7^- levels are known from the decay of Sb isotopes [15,16]. The lifetimes of 7^- and 10^+ levels in ^{132}Te were also measured in decay spectroscopy of mass-separated isomers [17,18] resulting in differing values for the 7^- level, compared to Ref. [16]. For the 4^+ and 8^+ levels no lifetime data exist in literature. In the present work, lifetimes have been measured for the low-lying yrast levels (2_1^+, 4_1^+, 6_1^+, 7_1^-, and 10^+) in the ^{130,132}Te nuclei, among which results for 4^+ levels are new.

II. EXPERIMENTAL DETAILS

The low-lying excited states of ^{130,132}Te have been populated from the combined routes of β^- decay of ^{130,132}Sb

*Corresponding author: btumpa@vecc.gov.in

 ©2022 American Physical Society

precursors and IT decay of higher-lying μs isomeric levels in these Te nuclei, viz. 10^+, 1.9 μs in ^{130}Te and 10^+, 3.7 μs in ^{132}Te. The neutron-rich Sb and Te isotopes were produced through thermal neutron-induced fission at Institut Laue-Langevin (ILL), Grenoble, France. A 0.13 mg/cm^2 ^{233}U target was used to produce $A = 130$ fragments and a 0.38 mg/cm^2 ^{235}U target to produce $A = 132$ fragments, respectively. The recoiling fission fragments were separated in mass and kinetic energy (65 MeV and 62 MeV, respectively) at an ionic charge state of 20^+ using the Lohengrin recoil fragment separator [19] and were detected with an ionization chamber (IC) placed at the focal plane. The IC provides a start signal for decay measurements of μs isomers. A parabola spectrometer such as Lohengrin has a degeneracy in A/q, i.e., depending on the q setting, different A with similar A/q may reach the focal plane. However, a parabola spectrometer is also a velocity filter, i.e., different A will have different kinetic energies $E \approx A$. Since the IC measures moreover E of every incoming fragment, the degeneracy can be resolved and different A can be identified. Obviously, the delayed β decays occur much later, outside the correlation window of the incoming ions. Therefore, delayed decays will show the whole A/q cocktail beam arriving in the focal plane.

An array of four 1.5″ × 1.5″ $LaBr_3$(Ce) detectors, kept at an angle of 90° with respect to each other, was used for the detection of deexciting γ radiations. The reason for using the most compact geometry for $LaBr_3$(Ce) detectors is to maximize the γ − ray efficiencies of the detectors. Target-to-detector distance was 2.2(2) cm and single-detector efficiency has been reported to be 3.7% at 122 keV of ^{152}Eu [20]. In addition, two Clover HPGe detectors were also placed near the focal plane for clean identification of γ rays from the separated fission fragments. The γ decays that followed the IT or β^- decays were selected through coincidence (IT) or anticoincidence (β^-), respectively, with IC, as the case may be.

The energy and time information from these detectors were obtained using the preamplifier outputs from the Clovers and the anode signals of the photomultiplier tubes (Hamamatsu 13435) connected to the $LaBr_3$ crystals. Time difference signals among any two $LaBr_3$ detectors were generated by constant fraction discriminators (Ortec 935), duplicated with logic FIFO modules and measured with time-to-amplitude converter (TAC) (Ortec 567) with a time range of 100 ns. All the signals were digitized with a VME-based 100 MHz digitizer (CAEN V1724) in triggerless mode storing the digital time stamp information for all the parameters event by event. The frequency or sampling rate of the digitizer module was sufficient to digitize the three types of parameters; (i) energy output from $LaBr_3$, (ii) energy signals from two Clovers, and (iii) TAC outputs.

The lifetimes were measured either (i) from the γ-γ coincidences among two $LaBr_3$ detectors when they are in anticoincidence with IC, therefore, ensuring that the γ rays are coming purely from β^- decays of Sb precursors or (ii) from the IC-Clover coincidence, which ensures that the γ rays are purely following the isomeric decay of the μs isomers in Te. The digitized TAC outputs with total range of 100 ns is suitable for fast timing measurements using generalized centroid difference (GCD) method [21] and slope method up to level lifetimes ≈30 ns. The slope method exploiting the $LaBr_3 - LaBr_3$ time stamp difference data of the digitizer was utilized for the measurement of level lifetimes, which are greater than 30 ns and up to few hundreds of nanoseconds. For the above two purposes, the β^-−decay events were considered owing to their higher statistics compared to the IT decay events and lifetime measurements were performed through $LaBr_3 - LaBr_3$ coincidences in anticoincidence with IC. On the contrary, lifetimes ≈ μs or more were measured using the time stamp difference data of delayed ion (IC)-γ (Clover) coincidences gathered from the digitizer, therefore, utilizing the IT decay events only. The data analysis for the extraction of nuclear level lifetimes has been carried out using the SoCo2 analysis package [22].

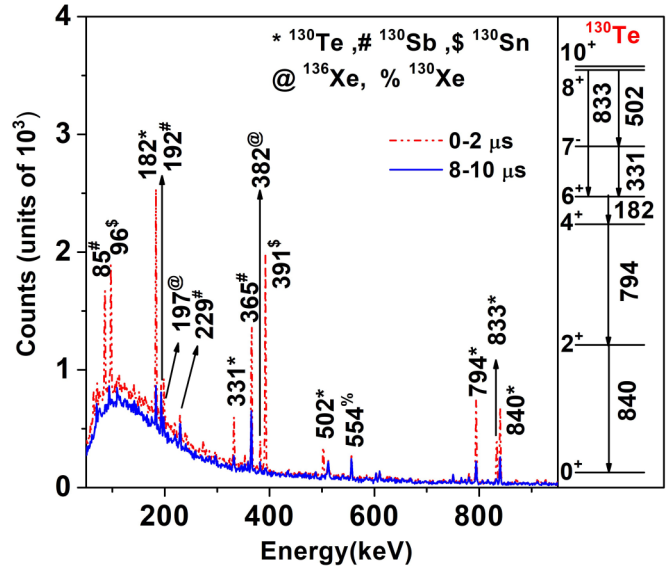

FIG. 1. The total energy projection from IC-Clover data for $A = 130$ within 0–2 μs after ion arrival (red) and 8–10 μs after ion arrival (blue). The γ lines arising from different isobars and their decay products are marked. γ rays from decay of the 10^+ level of ^{130}Te are shown on the right. The J^π values for the yrast levels are taken from Ref. [10].

III. RESULTS

The γ transitions from the decay of all the isobaric products and their daughters, which are deposited in the focal plane of Lohengrin, were studied from IC gated Clover projections. Spectra for $A = 130$ were obtained with a 2 μs wide coincidence time window, either directly after ion arrival (0–2 μs) or delayed compared to ion arrival (8–10 μs), are shown in Fig. 1. Similarly, spectra for $A = 132$ that were obtained with a 10 μs wide coincidence time window, either directly after ion arrival (0–10 μs) or delayed after ion arrival (70–80 μs), are shown in Fig. 2. One can clearly distinguish the rapidly decreasing γ transitions that are mainly populated by IT decay of short-lived μs isomers and the near-constant γ transitions that are populated in β decays. The 6^+ isomer in ^{136}Xe is very

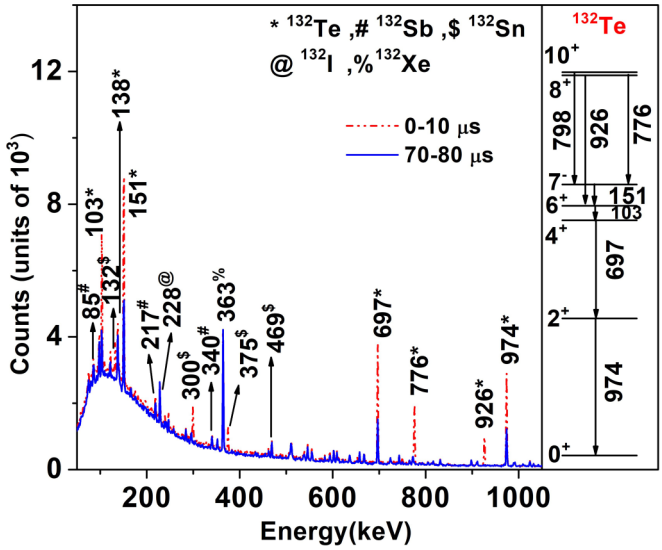

FIG. 2. The total energy projection from IC-Clover data for $A = 132$ within 0–10 μs after ion arrival (red) and 70–80 μs after ion arrival (blue). The γ lines arising from different isobars and their decay products are marked. γ rays from decay of the 10^+ level of ^{132}Te are shown on the right. The J^π values for the yrast levels are taken from Ref. [10].

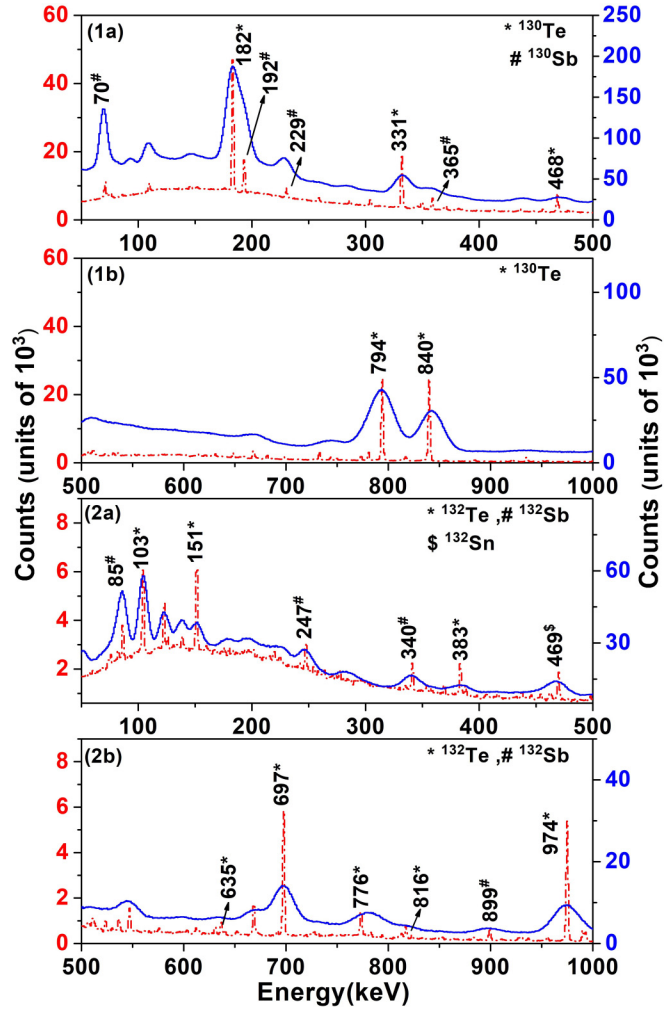

FIG. 3. The total energy projections are shown from 200 ns prompt $LaBr_3$-$LaBr_3$ and $LaBr_3$ – Clover coincidence events for $A = 130$ [(1a), (1b)] and $A = 132$ [(2a), (2b)]. In contrast to Fig. 1 and 2, here an antigate was applied for incoming ions, i.e., IT decays are suppressed and only β – delayed γ lines are observed. The strong γ lines of Te are seen with those from other neighboring isobars.

strongly populated in fission and due to a similar A/q ratio, the tail of ^{136}Xe appears in the IC spectrum of $A = 130$.

The γ rays of interest from ^{130,132}Te (shown at the right of Fig. 1 and Fig. 2) are clearly visible in these spectra along with other transitions from the neighboring isobars. The following sections describe the lifetime measurements in these two nuclei through GCD method (for 2^+ and 4^+ levels) and slope methods (for 6^+, 7^-m and 10^+ levels) utilizing $\gamma - \gamma$ coincidence from pure β^- decay events and ion-γ coincidence from pure IT decay events. The lifetimes of the 8^+ levels could not be measured as this level is fed by very low-energy γ rays, viz. 22 keV for ^{132}Te and 19 keV for ^{130}Te and the present setup was not equipped for the measurement of conversion electrons.

A. Lifetimes measurement with GCD method from β decay of ^{130,132}Sb

In GCD method, the difference of experimental centroid positions among the delayed and anti-delayed time distributions (ΔC_{exp}), generated for a particular γ-γ cascade, is measured [21]. Unless otherwise stated, the time difference distributions for different γ-γ cascades were generated using all combinations among the four $LaBr_3$ detectors in the setup. For this purpose, narrow energy gates, corresponding to the FWHM of a γ peak, were put on feeder and decay γ rays using prompt coincidence events gathered with $LaBr_3$ detectors in anticoincidence with the IC signals. The latter condition eliminates the γ rays from IT decay of the nuclei from the isobaric chain and, together with the prompt condition (200 ns coincidence window), reduces dead-time effects by at least one order of magnitude. The antigate applied in IC, as it suppresses the IT decays, allows us to see the pure β – delayed γ transitions that are used in the GCD analysis. The total projections from $LaBr_3$-$LaBr_3$ prompt coincidence events within a 200 ns coincidence time window are shown in Fig. 3. This is overlapped with the total projection of Clovers, generated with the same coincidence time window from $LaBr_3$ – Clover coincidence events, to understand the presence of contaminating transitions under any $LaBr_3$ peak to be used for the analysis.

The GCD method can also be ideally applied through fast timing analysis of pure IT decay data as well, for which it is a prerequisite to consider the IC-$LaBr_3$-$LaBr_3$ triple coincidence events. It has been verified that for Te nuclei with $A = 130$, 132; both $LaBr_3$-$LaBr_3$-$\overline{IC}$ and IC-$LaBr_3$-$LaBr_3$ coincidences provide consistent results. However, the former one has much higher statistics obtained with double coincidence of pure β – delayed γ rays from ^{130,132}Sb decay and so, wins over the higher purity generated with IT decay events

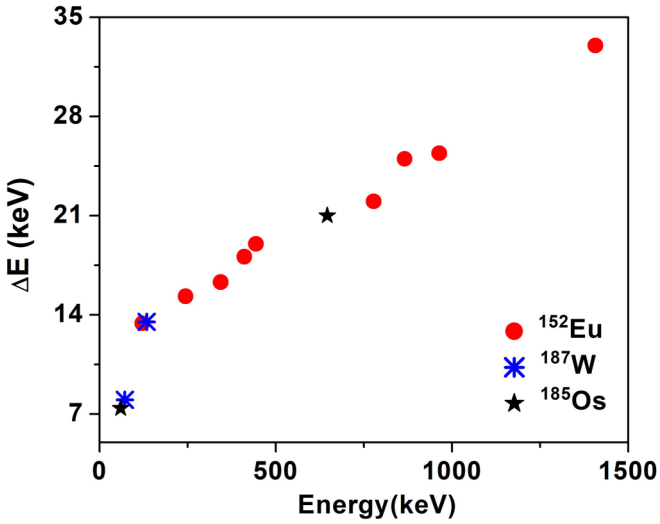

FIG. 4. The energy-dependent FWHM for the $LaBr_3$ setup used in the present experiment. The data points are obtained from the standard sources used in the experiment and are indicated.

from μs isomers. So, the γ-γ fast timing analysis obtained from the pure $\beta-$ delayed γ rays have been considered in the present work for the lifetime measurements through GCD method. In the present analysis, energy gates corresponding to different γ-γ cascades in ^{130,132}Te were put to generate the time difference distribution spectra. The gate widths were $\pm$10 keV about the peak positions at all energies except 103 (^{132}Te) and 182 (^{130}Te) keV for which $\pm$6 keV gates were used following the variation of FWHM as a function of γ energy, shown in Fig. 4.

Lifetimes well below the time resolution of the $LaBr_3/CeBr_3$ detectors and down to few picoseconds can be measured through this well-established GCD method [21,23]. The so-called centroid difference (ΔC_{exp}), corrected for the background contribution (t_{corr}), is used for the lifetime measurement when compared with the prompt response difference (PRD) of the setup, using the following relations:

$$\tau = \tfrac{1}{2}[\Delta C_{FEP} - PRD] \qquad (1)$$

$$\Delta C_{\mathrm{FEP}} = \Delta C_{\mathrm{exp}} + t_{\mathrm{corr}}\delta\tau = \frac{1}{2}\sqrt{(\delta\Delta C_{\mathrm{exp}})^2 + (\delta t_{\mathrm{corr}})^2 + (\delta PRD)^2}. \qquad (2)$$

The PRD value for each cascade is determined from the PRD curve, shown in Fig. 5, which has been generated using the time difference distributions of known γ-γ cascades from the decay of ^{152}Eu, ^{185}Os, and ^{187}W sources with the same $LaBr_3$ setup. The use of ^{185}Os and ^{187}W sources provided background-free very fast low-energy γ-γ and x-ray-γ coincidences as illustrated in Ref. [20]. Experimental data points were fitted with the PRD calibration function given in Ref. [20]. The PRD curve, so obtained for the present work, represents the variation of time walk as a function of γ energy of the present setup. The PRD is found to be well calibrated in the total dynamic range and is well within 200 ps even at very low energy. The PRD uncertainty $\delta PRD = 3$ ps, as seen from the fit residuum in Fig. 5(b), corresponding to the standard deviation of the experimental data to the fitted PRD curve, was considered while calculating the error in the measured lifetime following Eq. (1). The uncertainty in ΔC values depends on the statistics (n) gathered for a time difference distribution of any γ-γ cascade having a particular width ($\sigma = \frac{FWHM}{2.35}$) and is given by $\frac{\sigma}{\sqrt{n}}$.

Following the measurement of experimental centroid differences and the PRD, the background corrections (t_{corr}) were employed for determining the centroid differences corresponding to the full energy peak (FEP) (ΔC_{FEP}) that is free from any background contribution. The background correction is done following the prescription given in Ref. [20]. In this case, the particularity of the background is that it has a different time response compared to full energy peak events at the same energy. Furthermore, timing of feeding and decay γ rays are also different due to the variation in their energy. The following set of equations was used for the determination of t_{corr}, taking care of the Compton background underlying the FEPs (feeder and decay of a cascade) where

$$t_{\mathrm{corr}} = \frac{p/b(E_{\mathrm{decay}}).t_{\mathrm{corr}}(\mathrm{feeder}) + p/b(E_{\mathrm{feeder}}).t_{\mathrm{corr}}(\mathrm{decay})}{p/b(E_{\mathrm{feeder}}) + p/b(E_{\mathrm{decay}})};$$

$$t_{\mathrm{corr}}(\mathrm{feeder}) = \left[\frac{\Delta C_{\mathrm{exp}} - \Delta C_{BG}}{p/b}\right]_{\mathrm{feeder}}; \quad t_{\mathrm{corr}}(\mathrm{decay}) = \left[\frac{\Delta C_{\mathrm{exp}} - \Delta C_{BG}}{p/b}\right]_{\mathrm{decay}}.$$

The t_{corr} represent the total background correction that is necessary to be added to the raw centroid difference ΔC_{exp} and p/b represents the peak to background ratio. The ΔC_{BG} values for feeder and decay γ rays were obtained by fitting the background pattern surrounding the energy of interest in a particular cascade. This was done by taking the centroid differences corresponding to the coincidences among the photopeak of feeder (decay) and the Compton background neighboring to decay (feeder) γ rays. The p/b ratios corresponding to feeder and decay transitions are estimated from the corresponding gated projections of a particular cascade. The background corrections are associated with statistical uncertainties of ΔC values and the error in p/b ratios. This error is considered during the measurement of lifetime along with the errors in ΔC_{expt} and PRD following Eq, (1). Figures 6 and 7 represent the analyses for the extraction of level lifetimes, applied for 2_1^+ levels in ^{130,132}Te. These figures are used to demonstrate the measurement of two known

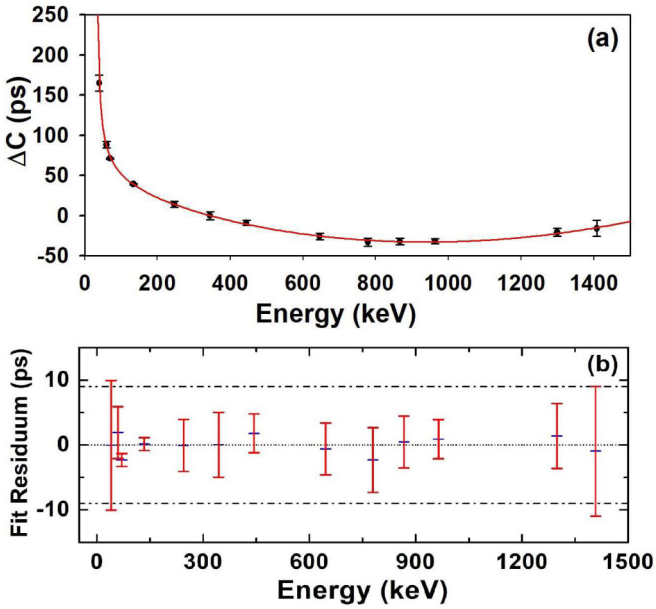

FIG. 5. (a) The prompt response difference (PRD) curve obtained for the present experiment showing the time walk distribution with γ − ray energy. (b) The fit residuum of PRD is shown with 3σ deviation shown with dot-dashed line. One σ has been considered for determining the error in level lifetime.

lifetimes through the GCD method, one in each of ^{130}Te and ^{132}Te. Different centroid difference values along with their errors, obtained from the analysis and relevant to the lifetime measurement are also indicated within the figures as well as in Table I. The uncertainties in the measurements can be followed from the gathered statistics (n) and width of the time difference distributions (σ) that are indicated on each figure. In case of ^{130}Te, the 794–840 keV coincidence was found to have no effect from the very weak 833 keV transition decaying from the 8^+ level as observed from Clover-$LaBr_3$ coincidences shown in Fig. 3(a) and Fig. 6. Both the lifetimes for the 2_1^+ levels of ^{130,132}Te were reasonably reproduced, as shown in Table II. Following the successful reproduction of known lifetimes, the lifetimes for the 4_1^+ levels of ^{130,132}Te were measured for which the results are shown in Fig. 8 and Fig. 9. For both these levels, low-energy transitions are involved and the results are first obtained with all combinations of $LaBr_3$ detectors and was also verified by excluding the combinations of neighboring detectors to avoid the effect of interdetector Compton scattering events [20]. In the latter analysis, the error is more owing to less statistics as the possibly problematic coincidence data among the neighboring detectors were excluded. The 182 ($6^+ \rightarrow 4^+$)–840 ($2^+ \rightarrow 0^+$) keV cascade was used, in case of ^{130}Te, instead of 182 ($6^+ \rightarrow 4^+$)–794 ($4^+ \rightarrow 2^+$) keV, resulting in the added lifetimes of the 2_1^+ and 4_1^+ levels. This is due to the observation that the 182 keV peak in the 794 keV gate is contaminated with the 192 keV γ line from ^{130}Sb decay. In this process, the lifetime of the 4_1^+ level was deduced to be 6(4) ps after subtracting the lifetime of the 2_1^+ level from the obtained result. This follows from the Bateman equations and the experimental procedure is called "absolute shift measurements," as has been introduced in Ref. [24]. The lifetime measured for this level was also deduced with exclusion of neighboring $LaBr_3$ pairs and the result comes out to be 8(4) ps (method 4 in Table I).

In case of ^{132}Te, the 103–697 keV cascade was used, which directly provided the lifetime of the 4_1^+ level as 60(5) ps by using all combinations of the four $LaBr_3$ detectors. However, as this cascade includes low-energy transition, this lifetime result was also verified excluding the combinations of neighboring $LaBr_3$ detectors and the analysis provides the lifetime of 55(5) ps for the 4_1^+ level of ^{132}Te. In addition, the added lifetime for 2_1^+ and 4_1^+ levels was also measured as 67(7) ps

TABLE I. Lifetime results (shown in bold) for low-lying levels of ^{130,132}Te using the GCD method. The quoted errors in the lifetimes are calculated considering the standard deviation (≈ 3 ps), obtained in the PRD curve and the errors estimated for the ΔC values. J^π values for the levels are taken from Ref. [10]. Three different ways are used to extract the lifetime for 4_1^+ level of ^{132}Te; (1) including all detectors and using cascade giving direct lifetime, (2) including all detectors and using cascade giving rise to added lifetime, and (3) excluding neighboring detector combinations and using cascade giving direct lifetime, (4) excluding neighboring detector combinations and using cascade giving rise to added lifetime. The adopted value is the average of results of 1 and 2. See text for details.

Nucleus	E_x (keV)	J^π	cascade (keV)	ΔC_{exp} (ps)	ΔC_{BG} (ps) (feeder)	p/b	ΔC_{BG} (ps) (decay)	p/b	t_{corr} (ps) (total)	ΔC_{FEP} (ps)	PRD (ps)	Lifetime (τ) (ps) Pres. work	Method*
^{130}Te	840	2_1^+	794–840	13(4)	27(12)	8.9(9)	31(13)	10.8(11)	−2(1)	11(4)	1	**5(3)**	1
	840,1633	$2_1^+ + 4_1^+$	182–840	68(3)	−99(10)	4.5(4)	309(15)	7.8(8)	12(4)	80(5)	58	**11(3)**	
	1633	4_1^+										**6(4)**	2
	840,1633	$2_1^+ + 4_1^+$	182–840	60(3)	−81(12)	5.8(1)	−244(12)	10.2(2)	26(2)	86(4)	58	**14(3)**	
	1633	4_1^+										**8(4)**	4
	1633	4_1^+										**6(4)**	adopted
^{132}Te	974	2_1^+	697–974	14(4)	39(8)	10.8(11)	−52(11)	16.7(17)	1(1)	15(4)	5	**5(3)**	1
	1671	4_1^+	103–697	136(5)	−173(19)	3.8(4)	−59(15)	5.1(5)	63(9)	199(10)	79	**60(5)**	1
	974, 1671	$2_1^+ + 4_1^+$	103–974	154(6)	−146(10)	3.7(4)	163(6)	12.8(13)	63(11)	217(13)	84	**67(7)**	
	1671	4_1^+										**62(8)**	2
	1671	4_1^+	103–697	137(5)	−162(14)	4.4(4)	−36(15)	5.5(6)	52(7)	189(9)	79	**55(5)**	3
	1671	4_1^+										**61(5)**	adopted

TABLE II. Lifetime results obtained in the present work for low-lying levels of ^{130,132}Te using the GCD method are compared with the existing literature values from fast timing measurements, Coulomb excitation (CE) measurements, and Doppler-shift attenuation method (DSAM). The literature value are either taken from direct measurements or deduced from $B(E2)$ values.

Nucleus	E_x (keV)	J^π	Presemt work Fast timing	Ref. [25] CE	Ref. [26] CE	Ref. [27] Fast timing	Ref. [28] CE	Ref. [29] CE	Ref. [30] CE	Ref. [31] DSAM
						(ps)				
^{130}Te	840	2_1^+	5(3)	3.3(1)			3.38(12)			
	1633	4_1^+	6(4)						4.7(10)	$1.395^{(+342+150)}_{(-239-124)}$
^{132}Te	974	2_1^+	5(3)		2.6(3)			$2.15^{(+25)}_{(-20)}$		
	1671	4_1^+	61(5)			<58				

using 103–974 keV cascade. Consequently, the lifetime for 4_1^+ level of ^{132}Te was measured to be 62(8) ps by subtracting the lifetime of 2_1^+ level [5(3) ps], as was done for ^{130}Te. In Table I, all the lifetimes measured through the GCD method are shown. For the 4_1^+ levels, the lifetimes have been measured with three different ways (1, 2, and 3) for ^{132}Te and in two different ways (2 and 4) for of ^{130}Te. All the results from different measurements are consistent with each other and the two out of these four methods (1 and 2) are independent measurements. The latter results could be used to find the adopted lifetime for the 4_1^+ level of ^{132}Te by averaging the resultant values.

The new results obtained in the present work for the 2_1^+ and 4_1^+ levels in ^{130,132}Te are compared with the existing data on measured lifetimes [25–27] in Table II. It is found that

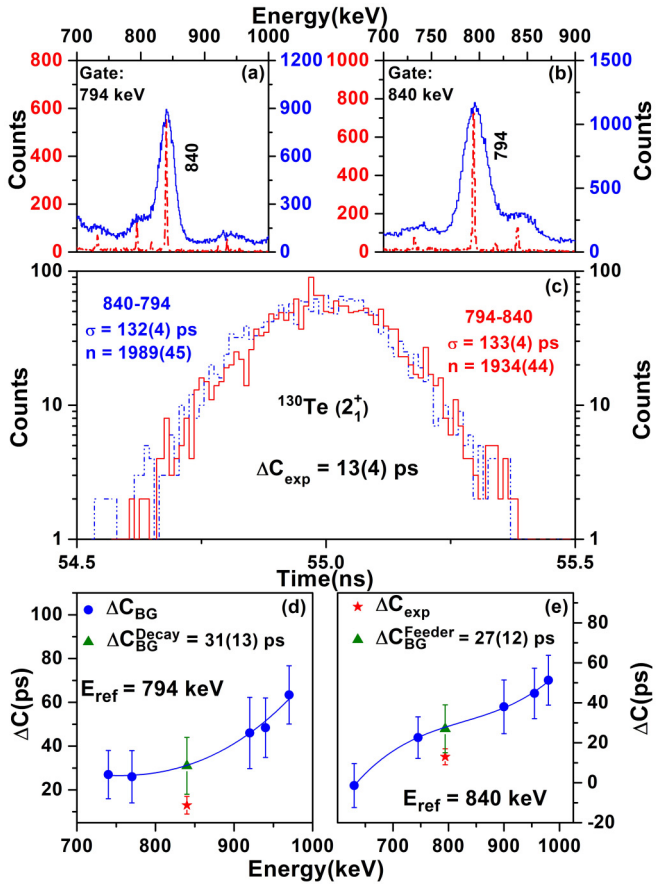

FIG. 6. The GCD analysis for the 2_1^+ level of ^{130}Te is shown. (a) and (b) show the energy gates corresponding to the 794–840 keV cascade from $LaBr_3$-$LaBr_3$ (solid blue) and $LaBr_3$ – Clover (dash-dotted red) coincidences; (c) shows the γ-γ delayed and antidelayed TACs for the measurement of the centroid difference. (d) and (e) show the background corrections obtained for decay and feeder, respectively.

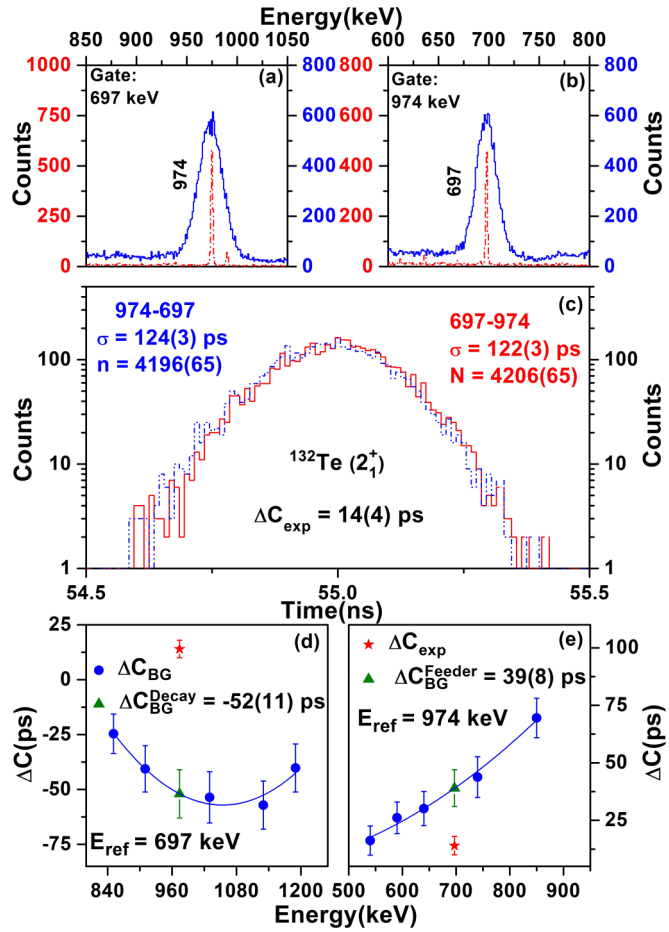

FIG. 7. The GCD analysis for the 2_1^+ level of ^{132}Te is shown. (a) and (b) shows the energy gates corresponding to the 697–974 keV cascade from $LaBr_3$-$LaBr_3$ (solid blue) and $LaBr_3$ – Clover (dash-dotted red) coincidences; (c) shows the γ-γ delayed and anti-delayed TACs for the measurement of the centroid difference. (d) and (e) show the background corrections obtained for decay and feeder, respectively.

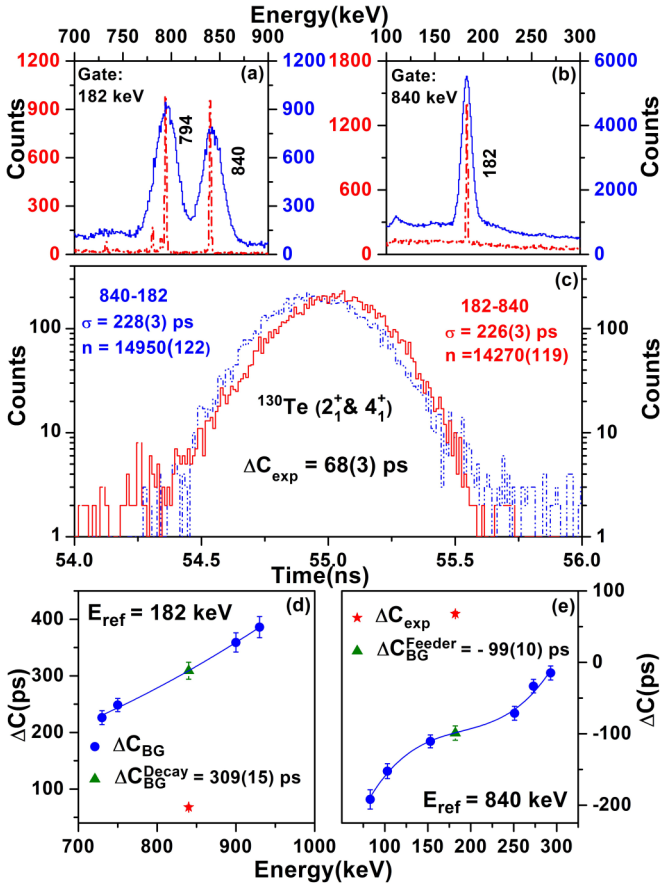

FIG. 8. The GCD analysis for the 4_1^+ level of ^{130}Te is shown. The results show the added lifetimes of 2^+ and 4^+ levels through GCD analysis of the 182–840 keV cascade. (a) and (b) show the energy gates as in Fig. 6 and 7; (c) shows the overlapped delayed and antidelayed TACs. (d) and (e) show the background analysis at 840 and 182 keV, respectively.

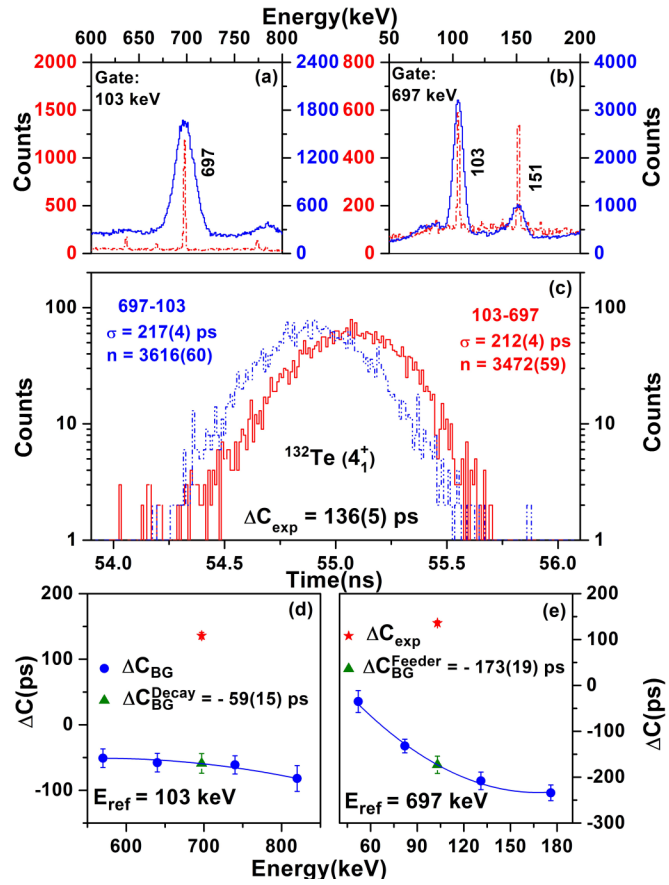

FIG. 9. The GCD analysis for the 4_1^+ level of ^{132}Te is shown. (a) and (b) show the energy gates corresponding to the 103–697 keV cascade as in Fig. 6 and 7; (c) shows the overlapped delayed and antidelayed TACs. (d) and (e) show the background analysis at 697 and 103 keV, respectively.

the lifetime data for the 4_1^+ level in ^{130,132}Te are obtained for the first time in the present work except an upper limit of lifetime for the 4_1^+ level in ^{132}Te is known from a preliminary measurement with centroid difference technique [27]. In addition, the lifetimes for the 2_1^+ and 4_1^+ levels of ^{130,132}Te could also be deduced from the $B(E2)$ values obtained in Coulomb excitation measurements [28–30]. The lifetimes of these levels, so obtained, come out to be 3.38(12) (^{130}Te, 2_1^+) [28], 4.7(10)(^{130}Te, 4_1^+) [30], and $2.15^{(+25)}_{(-20)}$(^{132}Te, 2_1^+) [29], respectively, and are shown in Table II. A very recent measurement with Doppler shift attenuation method is also found to be reported on 4_1^+ level in ^{130}Te [31].

B. Lifetime measurement with the slope method

The lifetimes can be measured by fitting the slope of the exponential decay curve of the respective γ rays obtained with $LaBr_3$ detectors when level lifetime is more than even a nanoseconds. Lifetimes were determined with slope fitting for few levels in ^{130,132}Te and two different types of analyses were done. These were obtained using the time difference distribution from (i) $\gamma(LaBr_3)$-$\gamma(LaBr_3)$ coincidence in anticoincidence with IC, therefore, taking purely the β^- decay of ^{130,132}Sb precursors into consideration and (ii) ion (IC)-γ (Clover) coincidences, so, purely considering the IT decay events. The time spectra of long-lived isomers, obtained in γ-γ or IC-γ analyses, only have extremely fast ($\ll 1$ ns) background contributions. It is absolutely unnecessary to remove this fast background contribution, since it has no effect on the slope [35]. Therefore, for all the levels, slopes of the γ-γ and IC-γ time projections, giving rise to direct time differences, were fitted with exponential decay functions without any kind of background subtraction. Except for 7^- level of ^{132}Te, clean slopes are obtained above the background due to decay of a single level and these slopes were fitted to obtain the level lifetimes. The two different analyses and corresponding results are given below.

1. γ-γ coincidence from β^- decay of ^{130,132}Sb

The exponential time dependence of the $\gamma(LaBr_3) - \gamma(LaBr_3)$ time difference distributions in anticoincidence with IC were fitted, to measure the lifetimes for the isomers with lifetime up to few hundreds of nanoseconds, where clean slopes were visible. In this measurement, pure β^- – delayed γ rays were considered and two different kinds of analyses were done for lifetime measurements: (i) time difference dis-

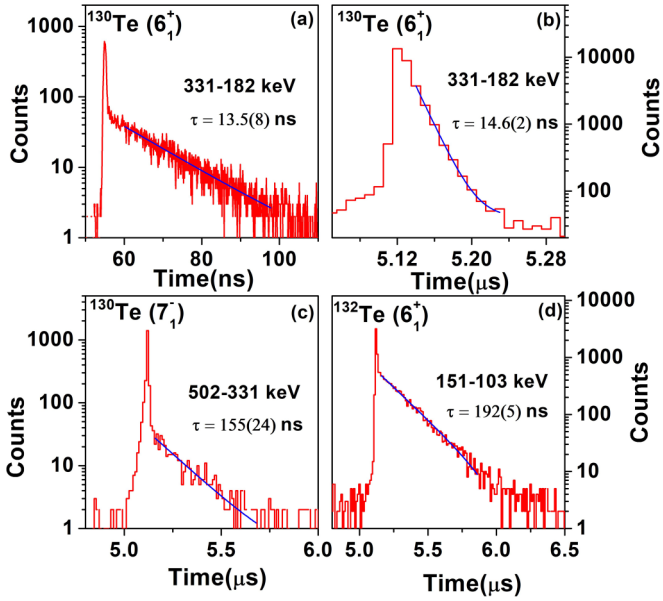

FIG. 10. The slope analysis for lifetimes in the nanoseconds range through γ-γ coincidence analysis using $LaBr_3$-$LaBr_3$ (a) TAC and (b), (c), (d) digital time stamp data. The 10 ps time per channel was used for the TAC data and the standard time per channel for DTS was 10 ns. The lifetime of the 6^+ level of ^{130}Te is reproduced within error from both the analysis.

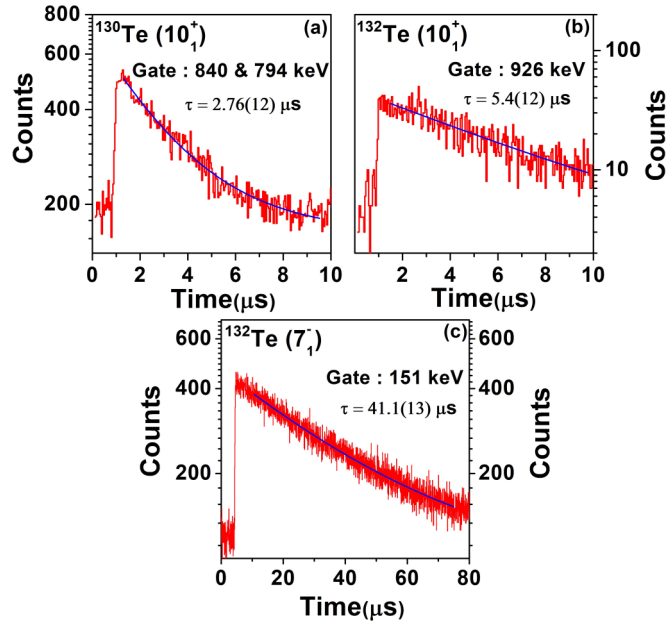

FIG. 11. The slope analysis for lifetimes in the microseconds range through IC-γ (Clover) coincidence analysis using digital time stamp information.

tribution was measured from the digitized TAC data. This was utilized to determine level lifetimes, which are less than ≈30 ns, viz. for the 6^+ level of ^{130}Te. (ii) Time difference information was taken from the digital time stamping (DTS). This was used for the cases where lifetimes are larger than 30 ns. The lifetimes for the 6^+ level of ^{132}Te and the 7^- level of ^{130}Te were measured with this analysis. As the DTS data is used for measurement of longer lifetimes, the 10 ns/channel calibration in DTS data was appropriate compared to the high-resolution 10 ps/channel used for TAC data. In order to demonstrate the consistency of both the methods, the lifetime of the 6^+ level of ^{130}Te was also deduced from DTS data along with the TAC data. It is observed that both the methods reproduce the lifetime quite consistently. The results from both the analysis are shown in Fig. 10 and details are given in Table III, in comparison to data available in existing literature.

2. *Ion-γ coincidence with IT decay of* ^{130,132}Te

The ion-γ coincidence has been used for lifetime measurements of the μsec isomers (10^+ levels in ^{130,132}Te and 7^- level in ^{132}Te) populated through the IT decay of ^{130,132}Te. For this purpose, time difference was analyzed from DTS data for IC-Clover coincidence events. The resultant time difference distributions are shown in Fig. 11 and tabulated in Table IV in comparison with the literature values. Pure slopes were obtained for the 10^+ levels and so, the lifetimes could be measured directly fitting the slope.

However, in the case of 7^- level of ^{132}Te, the time projection has a contribution from the feeding of the 10^+ isomeric level. So the obtained slope for this level (τ_{fit}) is the resultant of two contributions, one feeding from direct population of the 7^- (or short-lived precursors that decayed in flight) (N_{7^-}) and the other from the decay of the 10^+ level (N_{10^+}) with lifetime τ_{10^+}. Accordingly, the level lifetime for the 7^- level of ^{132}Te (τ_{7^-}) is determined from the fitted slope (τ_{fit}) following

TABLE III. Lifetime results (shown in bold) for the low-lying levels in ^{130,132}Te using the slope method from β decay of Sb precursors. Level energies have been quoted from Refs. [25,26]. J^π values for the levels are taken from Ref. [10].

Nucleus	E_x (keV)	J^π	gating cascade (keV)	gating condition	Lifetime τ (ns)	
					Present work	Lit.
^{130}Te	1815	6^+_1	331–182	$LaBr_3$-$LaBr_3$ TAC	**13.5(8)**	14.1(7) [25]
	1815	6^+_1	331–182	$LaBr_3$-$LaBr_3$ DTS	**14.6(2)**	
	2147	7^-_1	502–331	$LaBr_3$-$LaBr_3$ DTS	**155(24)**	159(7) [33], 166(11) [25], 268(16) [34]
	2649	8^+_1			**<120**	-
^{132}Te	1774	6^+_1	151–103	$LaBr_3$-$LaBr_3$ DTS	**192(5)**	209(11) [26]

TABLE IV. Lifetime results (shown in bold) for the low-lying levels in ^{130,132}Te using the slope method from IT decay. Level energies for 7^- and 10^+ levels in ^{132}Te have been quoted from Refs. [25,26]. The excitation energy for 10^+ level in ^{130}Te is quoted by averaging the values from Ref. [32] and Ref. [33]. J^π values for the levels are taken from Ref. [10].

Nucleus	E_x (keV)	J^π	gating γ transition (keV)	gating condition	Lifetime τ (μs)	
					Present work	Lit.
^{130}Te	2666	10^+_1	IC-(794+840)	IC-Clover DTS	**2.76(12)**	2.7(1) [25]
^{132}Te	1925	7^-_1	IC-151	IC-Clover DTS	**41.1(13)**	40.5(22) [26], $41.3^{(+17)}_{(-16)}$ [18]
	2701	8^+_1			**<1.2**	-
	2723	10^+_1	IC-926	IC-Clover DTS	**5.4(12)**	5.10(13) [18], 5.34(13) [26]

Eq. (3), given below, which is derived from the Bateman's prescription

$$\tau_{fit} = \frac{N_{10^+} \times [\tau_{10^+} + \tau_{7^-}] + N_{7^-} \times \tau_{7^-}}{N_{10^+} + N_{7^-}} = \frac{N_{10^+}}{N_{151}} \times \tau_{10^+} + \tau_{7^-}, \quad (3)$$

where N_{151} ($= N_{10^+} + N_{7^-}$) represents the total decay from the 7^- level and is measured from the area of the 151 keV γ line in the IC-gated Clover spectrum. The fractional feeding of the 10^+ level to the 7^- level (N_{10^+}) is measured from the efficiency and branching corrected area of the 776 keV transition.

The lifetimes of the 10^+ levels, in both ^{130,132}Te, have been obtained by selecting energy gates on γ rays decaying from lower-lying levels (8^+ in case of ^{132}Te and 2^+ and 4^+ in case of ^{130}Te). So, the measured lifetime corresponds to ($\tau_{8^+} + \tau_{10^+}$) in case of ^{132}Te and ($\tau_{2^+} + \tau_{4^+} + \tau_{6^+} + \tau_{8^+} + \tau_{10^+}$) for ^{130}Te. Lifetimes for all these levels, except the 8^+ and 10^+, are measured to be much lower than $\approx \mu s$, the maximum being for the 6^+ levels (13.5 ns in ^{130}Te and 192 ns for ^{132}Te). Accordingly, as the data for the 10^+ levels could be fitted with a clean single slope above the constant background, it may be conjectured that the lifetimes of the 8^+ levels are not comparable to the 10^+ levels and lie in the nanosecond region only. The lifetimes of the 8^+ levels may be assumed to be less than the uncertainties obtained in the slope measurements for the corresponding 10^+ levels, viz. < 120 ns and < 1.2 μsec, respectively, for ^{130}Te and ^{132}Te. Shell model calculations, as discussed in the following section, also predict lifetimes of a few ns and a few tens of ns, respectively, for the 8^+ levels in ^{130}Te and ^{132}Te.

IV. DISCUSSION

The $B(E2)$ transition probabilities corresponding to the decay of low-lying levels in ^{130,132}Te have been deduced from the measured lifetimes. For this purpose, the branching ratios for a particular level was taken from the ENSDF database [25,26] and the conversion coefficient for a particular transition was calculated using the BrIcc code [36]. The transition energies for $10^+ \rightarrow 8^+$ decay are very low giving rise to large conversion coefficients. This energy is 22 keV for ^{132}Te but for ^{130}Te, it is less known experimentally and has been taken as 19 keV following Ref. [32]. The 10^+ level in ^{132}Te is known to be decaying through a weak 798 keV $E3$ γ ray in addition to the 22 keV $E2$ transition. However, this weak branching having 2% relative intensity [10] has no significant effect on the $B(E2)$ transition probability for this level. As the measured lifetime has large errors and as the $B(E2)$ is a nonlinear function of lifetime, the progressive errors in $B(E2)$ values are expected to be asymmetric in nature and the same has been estimated following Ref. [37]. The experimental $B(E2)$ transition probabilities obtained in the present work for low-lying yrast levels in ^{130,132}Te are shown in Table V.

The $B(E2)$ transition probabilities for low-lying yrast levels in ^{130,132}Te are also shown in Fig. 12 in comparison with the neighboring Te isotopes around ^{132}Sn. It is observed that the measured $B(E2)$ values in the present work globally corroborate with measurements in neighboring isotopes [11,12,28–30] and reflect the expected double shell closure at ^{132}Sn. It is observed that the lifetime data for 4^+_1 level in ^{128}Te is missing in literature. However, $B(E2)(4^+_1 \rightarrow 2^+_1)$ transition probability for this nucleus is available from an exploratory analysis of the excited-state Coulomb excitation measurement [30]. Also, lifetime or $B(E2)$ data is not available for the 10^+ level in $N = 82$ ^{134}Te and it would be important to measure the same.

The large basis shell model calculations were performed, to interpret the level structure and the electromagnetic transition rates, using the NuShellX code [38]. The calculations have been performed distributing the proton and neutron particles above the ^{100}Sn core over the 50–82 subshell space. The considered model space was comprised of ($1g_{7/2}$, $2d_{5/2}$, $2d_{3/2}$, $3s_{1/2}$, $1h_{11/2}$) orbitals for both protons and neutrons. The calculations were carried out in full valence space without any truncation and using the *sn100pn* interaction [39], available with the code. Some details on interaction matrix elements and single-particle energies can also be found in Ref. [7]. The calculation is found to reproduce the experimental level energies quite well except the flipping of 8^+ and 10^+ energy levels in ^{132}Te and underestimation of 8^+ and 10^+ energy levels in

TABLE V. The experimental $B(E2)$ transition probabilities for the low-lying levels in ^{130,132}Te are shown.

Nucleus	$B(E2)(J^\pi_i \rightarrow J^\pi_f)$ (W.u.)				
	$2^+ \rightarrow 0^+$	$4^+ \rightarrow 2^+$	$6^+ \rightarrow 4^+$	$8^+ \rightarrow 6^+$	$10^+ \rightarrow 8^+$
^{130}Te	$10.0^{(+150)}_{(-40)}$	$11.0^{(+220)}_{(-40)}$	$6.4^{(+4)}_{(-4)}$	$>2.5 \times 10^{-4}$	$2.2^{(+1)}_{(-1)}$
^{132}Te	$4.7^{(+70)}_{(-18)}$	$2.0^{(+2)}_{(-1)}$	$3.6^{(+1)}_{(-1)}$	$>1.2 \times 10^{-5}$	$1.1^{(+3)}_{(-2)}$

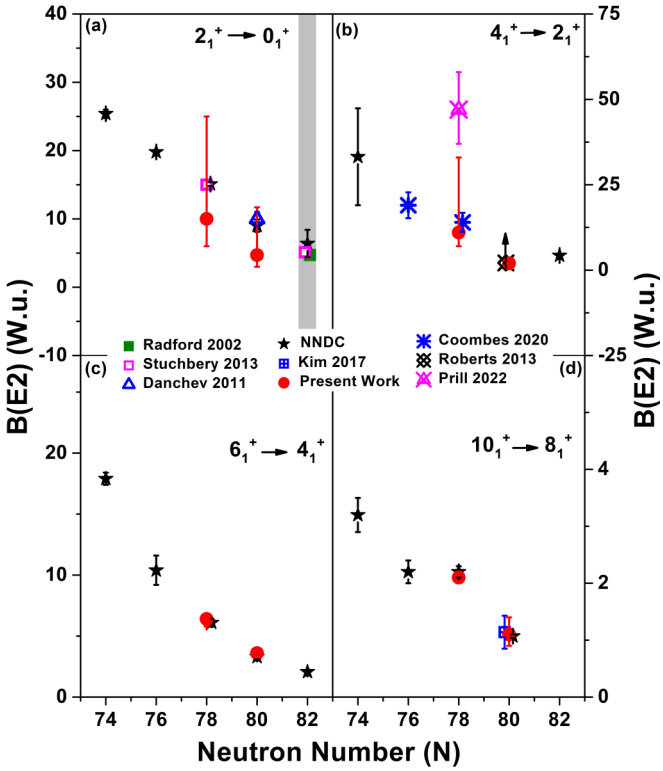

FIG. 12. The $B(E2)$ values for the decay of even spin positive parity levels in even mass Te nuclei as a function of neutron number. Several measurements exist for $B(E2)$ values through Coulomb excitation and lifetime measurements, viz. Radford 2002 [12], Stuchbery 2013 [28], Danchev 2011 [29], Coombes 2020 [30], Roberts 2013 [27], Kim 2017 [18], and Prill 2022 [31] that are also shown in the figure. The NNDC values are taken from Ref. [11] and for 10^+ decay in ^{132}Te $B(E2)$ value is deduced from the lifetime listed in ENSDF [26].

^{130}Te, as shown in Fig. 13. The difference between theory and experiment could be related to the interaction matrix elements used for the calculation and that may require reduction in the p-n interaction, as described in Ref. [40]. So, the calculation was also performed by reducing the p-n interaction matrix elements by a factor of 0.85 keeping the n-n (already reduced by factor 0.9 in *sn100pn*) and p-p interactions same as before and shown in Fig. 13 with Theory(mod.). It has been verified that the modified interaction could reproduce the order of 8^+ and 10^+ levels in ^{132}Te. However, this modification had almost no effect to the energies for the higher-lying levels (6^+ to 10^+) in ^{130}Te. The change in interaction matrix elements, therefore, needs to be looked into with a global perspective in this mass region and can be considered as a future perspective to the present work and other studies available in this mass region.

The decomposition of proton and neutron angular momenta contributing to each level was studied and the two most intense contributions in the total wave function are shown in Fig. 14(a) and Fig. 14(c), respectively, for ^{130}Te and ^{132}Te. It is found that the angular momenta of the 8^+ and 10^+ levels in ^{130,132}Te have major contribution from neutrons, 80% in case of ^{132}Te and 70% in case of ^{130}Te. However, mostly the protons contribute in the generation of angular momentum of the 6^+ and 4^+ levels. The 4^+ level in ^{132}Te is found to have 80% contribution from ($J_\pi = 4, J_\nu = 0$), which reduces to $\approx$ 50% in case of ^{130}Te. The 4^+ level in ^{130}Te is found to have considerable mixing with ($J_\pi = 2, J_\nu = 2$). The 2^+ levels in both the cases were found to have mixing among two contributions from ($J_\pi = 2, J_\nu = 0$) and ($J_\pi = 0, J_\nu = 2$). The 0^+ ground state of both the nuclei are found to have dominant ground state configurations of both proton and neutron with ($J_\pi = 0, J_\nu = 0$).

In Figs. 14(b) and 14(d), the major single-particle configurations in all the levels up to 10^+ of ^{130}Te and ^{132}Te, respectively, obtained with given *sn100pn* interaction are also shown. All those partitions having probability $>$ 5% are considered, wherever available, except in few cases. These plots demonstrate the amount of configuration mixing in the structure of these low lying levels in ^{130,132}Te. It is observed that the major configuration for these levels is $\pi g_{7/2}^2 \otimes \nu d_{3/2}^{-2} h_{11/2}^{-2}$ in ^{130}Te. Except for 8^+ and 10^+ levels, two major configurations, viz. $\pi g_{7/2}^2 \otimes \nu d_{3/2}^{-2}$ and $\pi g_{7/2}^2 \otimes \nu h_{11/2}^{-2}$ dominate the structure in ^{132}Te. In both the nuclei, 8^+ and 10^+ levels have almost pure configuration having the neutron holes in $\nu h_{11/2}$ orbital. In addition to the positive parity levels, the major configuration for the negative parity 7^- level has also been observed to be $\pi g_{7/2}^2 \otimes \nu d_{3/2}^{-1} h_{11/2}^{-3}$ in ^{130}Te and $\pi g_{7/2}^2 \otimes \nu d_{3/2}^{-1} h_{11/2}^{-1}$ in ^{132}Te with the angular momentum contribution coming from neutrons ($J_\pi = 0, J_\nu = 7$). Therefore, it may be concluded that for all the low-lying levels in ^{130,132}Te, only a few major single-particle configurations dominate the wave function indicating to a near spherical structures of these levels.

The $B(E2)$ transition probabilities for low-lying levels in ^{130,132}Te were calculated from shell model and are shown in Fig. 15, along with the experimental results, for all the yrast levels from 2_1^+ to 10_1^+. The decrease in the $B(E2)$ values with the increase in angular momentum could be related to less mixing of configurations for higher spin levels compared to the lower spin ones, as observed in Fig. 14.

In order to interpret the observed $B(E2)$ values for individual levels in ^{130,132}Te, the effective charge of both protons and neutrons were varied. The systematic shell model study of Ref. [41] shows that a variable neutron effective charge is required with the variation of neutron numbers in order to interpret the experimental data on the $B(E2)(0^+ \rightarrow 2^+)$ of Sn nuclei within N = 50–82. Similar changes may also be expected with the change in angular momentum, as different configurations, their mixing and the origin of the microscopic structure may change, as observed in case of ^{134}Te [28].

The transition probabilities in this mass region have often been calculated with increased effective charges for both proton and neutron, compared to the default value in NUSHELLX ($e^p = 1.5$, $e^n = 0.5$). These were based on the reproduction of $B(E2)$ values in even-even Sn, Te, and Ba isotopes [34,42,43]. In the present work, first the effective charges were tuned to reproduce the $B(E2)$ transition probabilities for the decay of 2^+ level in ^{134}Te ($Z = 52, N = 82$) and 10^+ decay in ^{130}Sn ($Z = 50, N = 80$). It is found that $e^p = 1.86$ reproduces the experimental data for 2_1^+ level in ^{134}Te and $e^n = 1.0$ is required to reproduce the value for 10^+ level decay

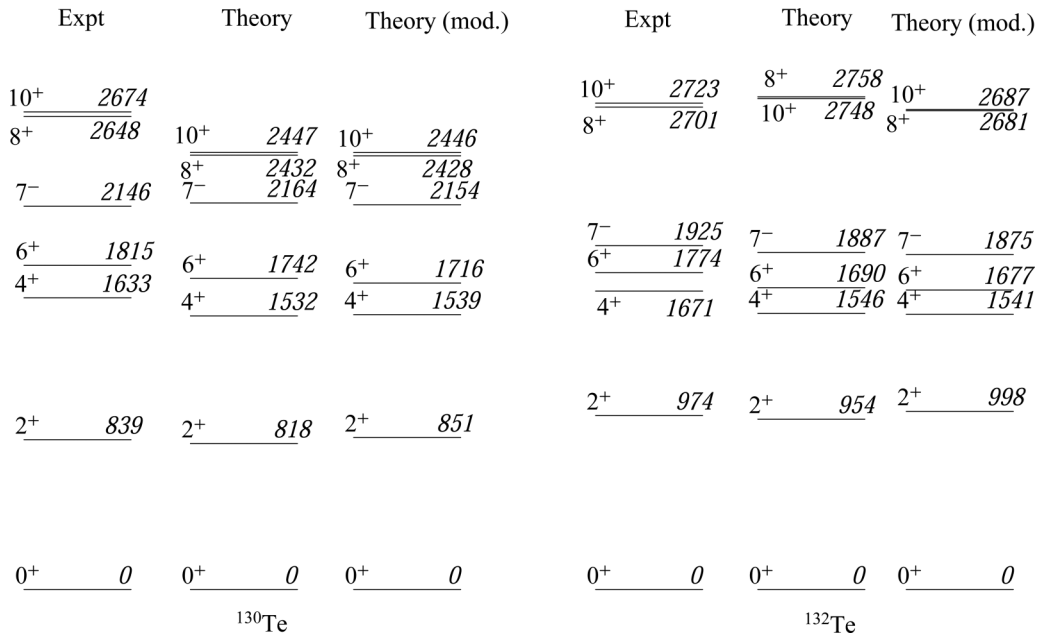

FIG. 13. The low-lying excited levels of ^{130,132}Te are compared to those calculated in the shell model. The levels marked with "Theory" shows the results obtained with *sn100pn* interaction without any modification and that with "Theory(mod.)" shows the results with reduced p-n interaction. The experimental level energies are taken from Refs. [25,26] except for the 10^+ state in ^{130}Te, for which the level energy is shown as 2666 keV taken as the average of the known values from Refs. [32,33].

in ^{130}Sn using *sn100pn* interaction. The transition probabilities in ^{130,132}Te, calculated with this tuned set of modified effective charges (ec1), are shown in Fig. 15. It is found that the increased proton and neutron effective charges can reproduce the experimental data, considering the errors, for most of the levels in ^{130}Te but greatly overestimate the experimental data in case of the ^{132}Te isotope with two neutron holes compared to $N = 82$ neutron shell closure, especially for the lower spin states.

It may be considered that in order to appropriately estimate the required effective charge for the low-lying levels of these nuclei (2^+, 4^+, 6^+), it would be important to find the neutron effective charge that is required to reproduce the experimental $B(E2)$ data for the above spin states in ^{130}Sn ($N = 80$) instead of 10^+. Moreover, in addition to the prescription for a variable neutron effective charge as a function of neutron number, it was shown in Ref. [41] that the isospin-dependent effective charge suggested by Bohr and Mottelson [44] ($e^n = 0.65$) reproduces the $B(E2)$ values in Sn nuclei near shell closure. The isospin-dependent effective charge for neutron was calculated in case of ^{130,132}Te also, following Eq. (1) of Ref. [41] and it comes out to be about 0.6 for both the nuclei. Interestingly, the present calculation with *sn100pn* interaction could also reproduce the $B(E2)(0^+ \rightarrow 2^+)$ of ^{130}Sn [45] with effective charge of 0.65. This finding on lower neutron effective charge for the low-lying levels in $N = 80$ Sn is also consistent with the quadrupole moment and deformation for the 2_1^+ levels in ^{126,128}Sn nuclei [46] that demands a lower effective charge for neutrons. Accordingly, the $B(E2)$ values for the low-lying levels in ^{130,132}Te were calculated with a reduced effective charge for neutron ($e^n = 0.65$), keeping $e^p = 1.86$ (ec2) and are shown on Fig. 15. This new set of effective charges, although it could reproduce the data much better than ec1, provided still higher result for 4_1^+ in ^{132}Te, which may be a result of higher effective charge of proton tuned with 2^+ in $N = 82$ Te.

Proton effective charge of $e^p = 1.5$ was found to reproduce the experimental $B(E2)$ values for 4^+ and 6^+ but not the 2^+ decays in ^{134}Te [28]. Consequently, default effective charges of $e^p = 1.5$, $e^n = 0.5$ (ec3) was used to calculate the transition probabilities in ^{130,132}Te. The default effective charge was found to reproduce some of the $B(E2)$ values in ^{130,132}Te quite reasonably, except the 6^+ levels, and a gross difference for $4^+ \rightarrow 2^+$ decay in ^{132}Te still remained in question.

In conclusion, although the systematics of $B(E2)$ values for individual levels are observed to fit in to the systematics of neighboring nuclei (Fig. 14), interesting discrepancies were observed for $B(E2)$ values in ^{132}Te during their interpretation through shell model calculations using higher effective charges, often used in this mass region. It is observed that ($e^p = 1.86$, $e^n = 0.65$) can reproduce the $B(E2)$ values quite reasonably for all the levels, except $4^+ \rightarrow 2^+$ decay in ^{132}Te. The effective charges were not tuned further below $e^p = 1.5$ and $e^n = 0.5$ and it was also found that the shell model results remain same even with reduced p-n interaction (factor = 0.85), as shown with ec3(mod.) in Fig. 15.

The $B(E2)$ values in $N = 78$, 80 Te could be related to the near spherical structure of these nuclei around ^{132}Sn, as also reflected in the shell model configurations of the associated levels. With addition of one valence proton to the semimagic ^{128}Sn ($N = 78$) core, the electric quadrupole strength in ^{129}Sb was found to be significantly enhanced [4] due to emerging

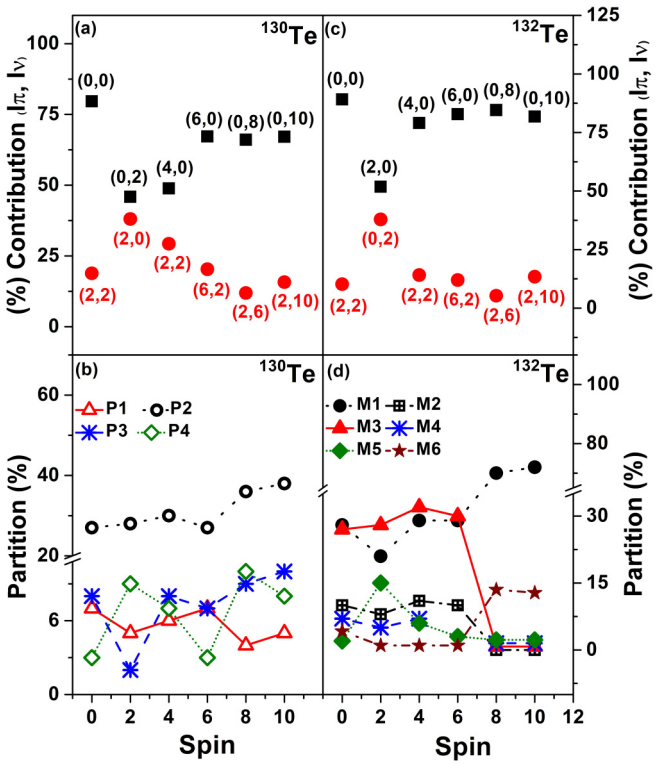

FIG. 14. The decomposition of angular momentum for the even spin positive parity levels are shown in (a) ^{130}Te and (c) ^{132}Te; the dominant single particle configurations obtained for different levels are shown in (b) ^{130}Te and (d) ^{132}Te; as obtained with shell model calculation. In (a) and (c), the black squares mark the major contribution and the red circle represents the minor contribution in the decomposed angular momentum of a level. In (b) and (d), the different configurations are marked as P1 ($\pi g^2_{7/2} \otimes \nu h^{-4}_{11/2}$), P2 ($\pi g^2_{7/2} \otimes \nu d^{-2}_{3/2} h^{-2}_{11/2}$), P3 ($\pi g^2_{7/2} \otimes \nu s^{-2}_{1/2} h^{-2}_{11/2}$), and P4 ($\pi g^2_{7/2} \otimes \nu d^{-1}_{3/2} s^{-1}_{1/2} h^{-2}_{11/2}$) in ^{130}Te and M1 ($\pi g^2_{7/2} \otimes \nu h^{-2}_{11/2}$), M2 ($\pi g^2_{7/2} \otimes \nu s^{-2}_{1/2}$), M3 ($\pi g^2_{7/2} \otimes \nu d^{-2}_{3/2}$), M4 ($\pi g^2_{7/2} \otimes \nu d^{-2}_{5/2}$), M5 ($\pi g^2_{7/2} \otimes \nu d^{-1}_{3/2} s^{-1}_{1/2}$), and M6 ($\pi d^2_{5/2} \otimes \nu h^{-2}_{11/2}$) in ^{132}Te.

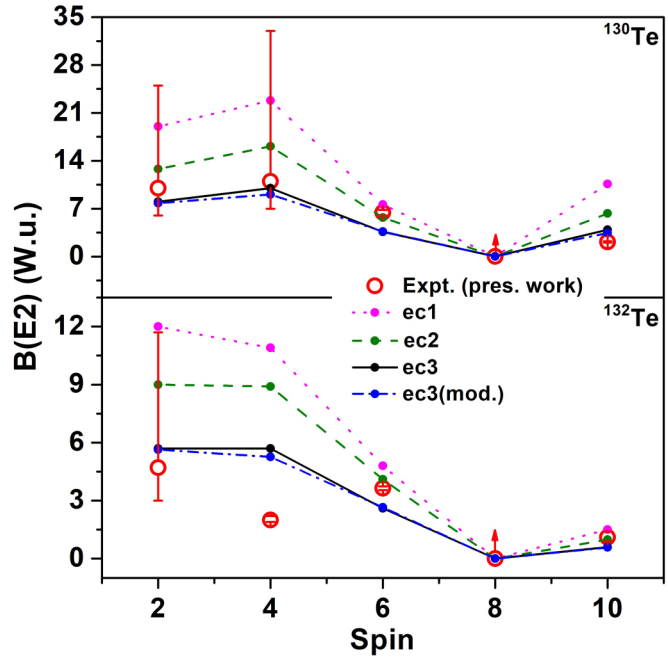

FIG. 15. The $B(E2)$ values for the decay of even spin positive parity levels in (a) ^{130}Te and (b) ^{132}Te nuclei as a function of angular momentum. The shell model results obtained in the present work are compared with the experimental data. The different sets of effective charges used for shell model calculations are indicated with ec1 ($e^p = 1.86, e^n = 1.0$), ec2 ($e^p = 1.86, e^n = 0.65$), and ec3 ($e^p = 1.5, e^n = 0.5$). ec3(mod.) represents the $B(E2)$ values obtained with the set of effective charge ec3 and modified p-n interaction. See text for details.

proton-neutron interaction compared to that in ^{128}Sn. On the contrary, with addition of one more proton in the structure of $N = 78$, 80 Sn, which have almost spherical structure as appears from the corresponding $E2$ matrix elements [46], the effect of neutron collectivity is reduced compared to neighboring Sb. This is expected as the residual proton-neutron interaction will be reduced in Te that has two protons in the $g_{7/2}$ orbital and neutron $h_{11/2}$ orbital almost filled. The excitation spectra and R_4 (E_{4^+}/E_{2^+}) ratios for ^{130,132}Te of 1.94 and 1.71, respectively, also confirm the same and designate their level structure to be vibrational in nature. The analogous $B(E2)$ ratios for the 4^+_1 and 2^+_1 decays are about 1.0 in ^{130}Te and <1.0 in ^{132}Te and confirms the near spherical structure.

The above interpretation for the $B(E2)$ values in ^{130,132}Te appears reasonable for all the levels, however, the very low $B(E2)$ for the $4^+ \rightarrow 2^+$ decay in ^{132}Te could be understood neither from its single-particle configuration nor from the effective charges. Similar variation in $B(E2)$ for different J levels was also observed in ^{134}Te [28] where the $B(E2)$ value for 2^+ level was on the higher side compared to that for the 4^+ and 6^+ levels. In ^{134}Te, the higher $B(E2)$ for 2^+_1 was explained with the contribution from coupling of valence proton particles to the vibration of ^{132}Sn core. It may be assumed that the variation in $B(E2)$ value for 4^+ level in ^{132}Te is also related to some other kind of excitations that could not be considered in the present shell model calculation. As the proton effective charge of 1.5 and neutron effective charge of 0.5 could reproduce the $B(E2)$ value for $4^+ \rightarrow 2^+$ level in ^{134}Te, it may also be assumed that deviation in $B(E2)(4^+ \rightarrow 2^+)$ in ^{132}Te is not related to proton but to neutron excitation.

It is observed that similar discrepancies with shell model and experimental data also exist for 4^+_1 level in ^{136}Te [47], which lies symmetrically on the other side of $N = 82$ shell closure of ^{132}Sn. So, deviation of experimental $B(E2)$ from the microscopic structure calculations is observed for 4^+_1 level in both $N = 80$ and 84 Te, one with two valence neutron holes and the other with two valence neutron particles with respect to the ^{132}Sn core. It is known that most of the levels in ^{132}Sn core correspond to particle-hole excitations across the $N = 82$ shell gap [48]. The 4^+_1 level in ^{132}Sn is originated with one neutron particle excited across $N = 82$ to the $\nu f_{\frac{7}{2}}$ orbital coupled to one neutron hole remaining below $N = 82$ in $\nu h_{\frac{11}{2}}$ orbital. So, the consideration of cross shell neutron excitations across $N = 82$ may help in explaining the discrepant $B(E2)$ value in both ^{132}Te and ^{136}Te.

However, the model space (*jj55pna*) used in the present shell model calculation considers orbitals in the 50–82 subshell space and do not include single-particle $f_{\frac{7}{2}}$ orbital beyond $N = 82$. So, the present calculation is not capable of considering such core excitations of neutron particles across $N = 82$ and, so, to confirm if any such contribution is involved in the structure of 4_1^+ level of ^{132}Te. Similarly the model space used in Ref. [47] considered neutrons only above $N = 82$ and the excitations across $N = 82$ could not be considered in their calculation. It might be important to perform a systematic shell model calculation using a model space involving cross shell excitations of neutrons, i.e., with a new model space involving higher-lying orbitals from 50–82 subshell space ($s_{\frac{1}{2}}$, $d_{\frac{3}{2}}$, $h_{\frac{11}{2}}$) below $N = 82$ and lower-lying orbitals from 82–126 subshell space ($f_{\frac{7}{2}}$) above $N = 82$, in order to understand this particular issue. This is a quite involved task [49] and can be taken up as a future perspective to the present work.

V. SUMMARY

The lifetimes have been measured for the low-lying levels in ^{130,132}Te among which the results for 4_1^+ levels are obtained for the first time, except an upper limit of lifetime is known for 4_1^+ in ^{132}Te from a very preliminary measurement. The transition strengths corresponding to the decay from these levels are studied and the present results in ^{130,132}Te corroborate with the systematics around the doubly closed ^{132}Sn. The microscopic origin of the low-lying levels in $N = 80$, 82 Te were studied comparing the experimental level energies and transition probabilities with that obtained from a large basis shell model calculation using unrestricted model space. It is observed that the structures of these levels solely correspond to single-particle excitations of the valence particles (proton) and holes (neutron) to the available orbitals in the 50–82 subshell space. The wave functions and $B(E2)$ values indicate that almost pure single-particle microscopic structures are involved in the excitation of all the levels with small change in configuration mixing as a function of angular momentum and suggest near spherical structures for all the low-lying levels. However, $B(E2)(4_1^+ \rightarrow 2_1^+)$ in ^{132}Te, with two valence neutron holes, could not be explained with the microscopic structure suggested by shell model, as was also observed for 4_1^+ level in ^{136}Te with two valence neutron particles. It is found necessary to explore the effect of particle-hole excitation of the ^{132}Sn core in the structure of this level in both ^{132}Te and ^{136}Te.

ACKNOWLEDGMENTS

Authors acknowledge Prof. M. Saha Sarkar for many fruitful scientific discussions regarding the shell model calculation and other physics issues in this mass region. The effort of the staffs of ILL is acknowledged for providing a good quality setup for the experiments. D.K. and T.B. gratefully acknowledge all support from VECC, DAE towards performing the experiment at an international laboratory. L.M.F. acknowledges the support from the Spanish government through RTI2018-098868-B-I00 project.

[1] V. Vaquero, A. Jungclaus, P. Doornenbal, K. Wimmer, A. Gargano, J. A. Tostevin, S. Chen, E. Nacher, E. Sahin, Y. Shiga *et al.*, Phys. Rev. Lett. **118**, 202502 (2017).

[2] Z. Q. Chen, Z. H. Li, H. Hua, H. Watanabe, C. X. Yuan, S. Q. Zhang, G. Lorusso, S. Nishimura, H. Baba, F. Browne, G. Benzoni, K. Y. Chae, F. C. L. Crespi, P. Doornenbal, N. Fukuda, G. Gey, R. Gernhäuser, N. Inabe, T. Isobe, D. X. Jiang *et al.*, Phys. Rev. Lett. **122**, 212502 (2019).

[3] C. Gorges, L. V. Rodríguez, D. L. Balabanski, M. L. Bissell, K. Blaum, B. Cheal, R. F. Garcia Ruiz, G. Georgiev, W. Gins, H. Heylen, A. Kanellakopoulos, S. Kaufmann, M. Kowalska, V. Lagaki, S. Lechner, B. Maaß, S. Malbrunot-Ettenauer, W. Nazarewicz, R. Neugart, G. Neyens, W. Nörtershäuser *et al.*, Phys. Rev. Lett. **122**, 192502 (2019).

[4] T. J. Gray, J. M. Allmond, A. E. Stuchbery, C.-H. Yu, C. Baktash, A. Gargano, A. Galindo-Uribarri, D. C. Radford, J. C. Batchelder, J. R. Beene, C. R. Bingham, L. Coraggio, A. Covello, M. Danchev, C. J. Gross, P. A. Hausladen, N. Itaco, W. Krolas, J. F. Liang, E. Padilla-Rodal *et al.*, Phys. Rev. Lett. **124**, 032502 (2020).

[5] J. M. Allmond, A. E. Stuchbery, C. Baktash, A. Gargano, A. Galindo-Uribarri, D. C. Radford, C. R. Bingham, B. A. Brown, L. Coraggio, A. Covello, M. Danchev, C. J. Gross, P. A. Hausladen, N. Itaco, K. Lagergren, E. Padilla-Rodal, J. Pavan, M. A. Riley, N. J. Stone, D. W. Stracener, R. L. Varner, and C. H. Yu, Phys. Rev. Lett. **118**, 092503 (2017).

[6] D. Rosiak, M. Seidlitz, P. Reiter, H. Naïdja, Y. Tsunoda, T. Togashi, F. Nowacki, T. Otsuka, G. Colò, K. Arnswald, T. Berry, A. Blazhev, M. J. G. Borge, J. Cederkäll, D. M. Cox, H. DeWitte, L. P. Gaffney, C. Henrich, R. Hirsch, M. Huyse, A. Illana, K. Johnston, L. Kaya, T. Kroll, M. L. Benito, J. Ojala, J. Pakarinen, M. Queiser, G. Rainovski, J. A. Rodriguez, B. Siebeck, E. Siesling, J. Snall, P. VanDuppen, A. Vogt, M. vonSchmid, N. Warr, F. Wenander, K. O. Zell, Phys. Rev. Lett. **121**, 252501 (2018).

[7] S. S. Alam, T. Bhattacharjee, D. Banerjee, A. Saha, S. Das, M. S. Sarkar, and S. Sarkar, Phys. Rev. C **99**, 014306 (2019).

[8] S. Ilieva, Th. Kröll, J. M. Régis, N. Saed-Samii, A. Blanc, A. M. Bruce, L. M. Fraile, G. de France, A.-L. Hartig, C. Henrich, A. Ignatov, M. Jentschel, J. Jolie, W. Korten, U. Köster, S. Lalkovski, R. Lozeva, H. Mach, N. Mărginean, P. Mutti, V. Paziy, P. H. Regan *et al.*, Phys. Rev. C **94**, 034302 (2016).

[9] E. S. Paul, P. J. Woods, T. Davinson, R. D. Page, P. J. Sellin, C. W. Beausang, R. M. Clark, R. A. Cunningham, S. A. Forbes, D. B. Fossan, A. Gizon, J. Gizon, K. Hauschild, I. M. Hibbert, A. N. James, D. R. LaFosse, I. Lazarus, H. Schnare, J. Simpson, R. Wadsworth *et al.*, Phys. Rev. C **51**, 78 (1995).

[10] J. Genevey, J. A. Pinston, C. Foin, M. Rejmund, R. F. Casten, H. Faust, and S. Oberstedt, Phys. Rev. C **63**, 054315 (2001).

[11] https://www.nndc.bnl.gov/ensdf/.

[12] D. C. Radford, C. Baktash, J. R. Beene, B. Fuentes, A. Galindo-Uribarri, C. J. Gross, P. A. Hausladen, T. A. Lewis, P. E.

Mueller, E. Padilla, D. Shapira, D. W. Stracener, C.-H. Yu, C. J. Barton, M. A. Caprio, L. Coraggio, A. Covello, A. Gargano, D. J. Hartley, and N. V. Zamfir, Phys. Rev. Lett. **88**, 222501 (2002).

[13] J. Terasaki, J. Engel, W. Nazarewicz, and M. Stoitsov, Phys. Rev. C **66**, 054313 (2002).

[14] C. J. Barton, M. A. Caprio, D. Shapira, N. V. Zamfir, D. S. Brenner, R. L. Gill, T. A. Lewis, J. R. Cooper, R. F. Casten, C. W. Beausang, R. Krücken, and J. R. Novak, Phys. Lett. B **551**, 269 (2003).

[15] A. Kerek, P. Carlé, and J. McDonald, Nucl. Phys. A **198**, 466 (1972).

[16] J. McDonald and A. Kerek, Nucl. Phys. A **206**, 417 (1973).

[17] K. Sistemich, W.-D. Lauppe, H. Lawin, F. Schussler, J. P. Bocquet, E. Monnand, and J. Blomqvist, Z. Phys. A **292**, 145 (1979).

[18] Y. H. Kim, A. Lemasson, M. Rejmund, A. Navin, S. Biswas, C. Michelagnoli, I. Stefan, R. Banik, P. Bednarczyk, S. Bhattacharya, S. Bhattacharyya, E. Clément, H. L. Crawford, G. De France, P. Fallon, J. Goupil, B. Jacquot, H. J. Li, J. Ljungvall, A. O. Macchiavelli *et al.*, Eur. Phys. J. A **53**, 162 (2017).

[19] P. Armbruster, M. Asghar, J. P. Bocquet, R. Decker, H. Ewald, J. Greif, E. Moll, B. Pfeiffer, H. Schrader, F. Schussler, G. Siegert, and H. Wollnik, Nucl. Instr. Meth. **139**, 213 (1976).

[20] J.-M. Régis, A. Esmaylzadeh, J. Jolie, V. Karayonchev, L. Knafla, U. Köster, Y. H. Kim, and E. Strub, Nucl. Instr. Meth. Phys. Res. Sect. A **955**, 163258 (2020).

[21] J.-M. Régis, N. Saed-Samii, M. Rudigier, S. Ansari, M. Dannhoff, A. Esmaylzadeh, C. Fransen, R.-B. Gerst, J. Jolie, V. Karayonchev, C. Müller-Gatermann, and S. Stegemann, Nucl. Instr. Meth. Phys. Res. Sect. A **823**, 72 (2016).

[22] N. Saed-Samii, git clone, https://gitlab.ikp.uni-koeln.de/nima/git/soco-v2.git.

[23] S. S. Alam, T. Bhattacharjee, D. Banerjee, A. Saha, Deepak Pandit, D. Mondal, S. Mukhopadhyay, Surajit Pal, P. Bhaskar, S. K. Das, and S. R. Banerjee, Nucl. Instr. Meth. Phys. Res. Sect. A **874**, 103 (2017).

[24] H. Mach, F. K. Wohn, G. Molnár, K. Sistemich, John C. Hill, M. Moszyński, R. L. Gill, W. Krips, and D. S. Brenner, Nucl. Phys. A **523**, 197 (1991).

[25] B. Singh, Nucl. Data Sheets **93**, 33 (2001).

[26] Yu. Khazov, A. A. Rodionov, S. Sakharov, and B. Singh, Nucl. Data Sheets **104**, 497 (2005).

[27] O. J. Roberts, A. M. Bruce, F. Browne, N. Mărginean, T. Alexander, T. Alharbi, D. Bucurescu, D. Deleanu, D. Delion, D. Filipescu, L. Fraile, I. Gheorghe, D. Ghiţă, T. Glodariu, D. Ivanova, S. Kisyov, R. Mărginean, P. J. R. Mason, C. Mihai, K. Mulholland, A. Negret *et al.*, P-and Acta Phys. Pol. B **44**, 403 (2013).

[28] A. E. Stuchbery, J. M. Allmond, A. Galindo-Uribarri, E. Padilla-Rodal, D. C. Radford, N. J. Stone, J. C. Batchelder, J. R. Beene, N. Benczer-Koller, C. R. Bingham, M. E. Howard, G. J. Kumbartzki, J. F. Liang, B. Manning, D. W. Stracener, and C.-H. Yu, Phys. Rev. C **88**, 051304(R) (2013).

[29] M. Danchev, G. Rainovski, N. Pietralla, A. Gargano, A. Covello, C. Baktash, J. R. Beene, C. R. Bingham, A. Galindo-Uribarri, K. A. Gladnishki, C. J. Gross, V. Yu. Ponomarev, D. C. Radford, L. L. Riedinger, M. Scheck, A. E. Stuchbery, J. Wambach, C.-H. Yu, and N. V. Zamfir, Phys. Rev. C **84**, 061306(R) (2011).

[30] B. J. Coombes, A. E. Stuchbery, J. M. Allmond, A. Gargano, J. T. H. Dowie, G. Georgiev, M. S. M. Gerathy, T. J. Gray, T. Kibédi, G. J. Lane, B. P. McCormick, A. J. Mitchell, N. J. Spinks, and B. P. E. Tee, EPJ Web Conf. **232**, 04003 (2020).

[31] S. Prill, A. Bohn, V. Everwyn, G. Häfner, F. Heim, M. Spieker, M. Weinert, J. Wilhelmy, and A. Zilges, Phys. Rev. C **105**, 034319 (2022).

[32] R. Broda, B. Fornal, W. Królas, T. Pawlat, J. Wrzesiński, D. Bazzacco, G. de Angelis, S. Lunardi, and C. Rossi-Alvarez, Eur. Phys. J. A **20**, 145 (2003).

[33] A. Astier, M.-G. Porquet, Ts. Venkova, Ch. Theisen, G. Duchêne, F. Azaiez, G. Barreau, D. Curien, I. Deloncle, O. Dorvaux, B. J. P. Gall, M. Houry, R. Lucas, N. Redon, M. Rousseau, and O. Stézowski, Eur. Phys. J. A **50**, 2 (2014).

[34] J. J. Valiente-Dobón, P. H. Regan, C. Wheldon, C. Y. Wu, N. Yoshinaga, K. Higashiyama, J. F. Smith, D. Cline, R. S. Chakrawarthy, R. Chapman, M. Cromaz, P. Fallon, S. J. Freeman, A. Görgen, W. Gelletly, A. Hayes, H. Hua, S. D. Langdown, I. Y. Lee, X. Liang *et al.*, Phys. Rev. C **69**, 024316 (2004).

[35] K. E. G. Löbner, in *The Electromagnetic Interaction in Nuclear Spectroscopy*, edited by W. D. Hamilton (North-Holland, New York, 1975).

[36] T. Kibédi, T. W. Burrows, M. B. Trzhaskovskaya, P. M. Davidson, and C. W. Nestor Jr., Nucl. Instr. Meth. Phys. Res. Sect. A **589**, 202 (2008).

[37] R. Barlow, in *Proceedings of the Statistical Problems in Particle Physics, Astrophysics, and Cosmology (PHYSTAT)*, Stanford, 2003, edited by R.P. Mount and , R. Reitmeyer, eConf C030908, 250 (2003); arXiv:physics/0401042 [physics.data-an].

[38] B. A. Brown and W. D. M. Rae, Nucl. Data Sheets **120**, 115 (2014).

[39] B. A. Brown, N. J. Stone, J. R. Stone, I. S. Towner, and M. Hjorth-Jensen, Phys. Rev. C **71**, 044317 (2005).

[40] S. Biswas, R. Palit, A. Navin, M. Rejmund, A. Bisoi, M. S. Sarkar, S. Sarkar, S. Bhattacharyya, D. C. Biswas, M. Caamaño, M. P. Carpenter, D. Choudhury, E. Clement, L. S. Danu, O. Delaune, F. Farget, G. deFrance, S. S. Hota, B. Jacquot, A. Lemasson, S. Mukhopadhyay, V. Nanal, R. G. Pillay, S. Saha, J. Sethi, P. Singh, P. C. Srivastava, S. K. Tandel, Phys. Rev. C **93**, 034324 (2016).

[41] T. Bäck, C. Qi, B. Cederwall, R. Liotta, F. Ghazi Moradi, A. Johnson, R. Wyss, and R. Wadsworth, Phys. Rev. C **87**, 031306(R) (2013).

[42] A. Vogt, B. Birkenbach, P. Reiter, A. Blazhev, M. Siciliano, K. Hadyńska-Klek, J. J. Valiente-Dobón, C. Wheldon, E. Teruya *et al.*, Phys. Rev. C **95**, 024316 (2017).

[43] M. Rejmund, A. Navin, S. Biswas, A. Lemasson, M. Caamaño, E. Clément, O. Delaune, F. Farget, G. de France, B. Jacquot, and P. Van Isacker, Phys. Lett. B **753**, 86 (2016).

[44] A. Bohr and B. Mottelson, *Nuclear Structure* (Benjamin, New York, 1975), Vol. II, Chap. 6, p. 515.

[45] B. Pritychenko, M. Birch, B. Singh, and M. Horoi, Atom. Data & Nucl. Data Tables **107**, 1 (2016).

[46] J. M. Allmond, D. C. Radford, C. Baktash, J. C. Batchelder, A. Galindo-Uribarri, C. J. Gross, P. A. Hausladen, K. Lagergren, Y. Larochelle, E. Padilla-Rodal, and C.-H. Yu, Phys. Rev. C **84**, 061303(R) (2011).

[47] G. Häfner, R. Lozeva, H. Naïdja, M. Lebois, N. Jovančević, D. Thisse, D. Etasse, R. L. Canavan, M. Rudigier, J. N. Wilson *et al.*, Phys. Rev. C **103**, 034317 (2021).

[48] J. Benito, L. M. Fraile, A. Korgul, M. Piersa, E. Adamska, A. N. Andreyev, R. Álvarez-Rodríguez, A. E. Barzakh, G. Benzoni, T. Berry *et al.*, Phys. Rev. C **102**, 014328 (2020).

[49] S. Das and M. S. Sarkar, Nucl. Phys. A **1014**, 122262 (2021).